TU Delft

Delft University of Technology

Holistic Processing of Sawdust to Enable Sustainable Hybrid Li-Ion Capacitors

Guo, Xiaoyang; van de Kleut, Dick; Zhang, Jia; Chen, Chaofan; Wang, Xuehang; Zheng, Tianye; Boles, Steven

DOI
10.1007/s11837-024-06542-1

Publication date
2024

Document Version
Final published version

Published in
JOM

Citation (APA)
Guo, X., van de Kleut, D., Zhang, J., Chen, C., Wang, X., Zheng, T., & Boles, S. (2024). Holistic Processing of Sawdust to Enable Sustainable Hybrid Li-Ion Capacitors. *JOM*, *76*(7), 3557-3566. https://doi.org/10.1007/s11837-024-06542-1

Important note
To cite this publication, please use the final published version (if applicable).
Please check the document version above.

Copyright
Other than for strictly personal use, it is not permitted to download, forward or distribute the text or part of it, without the consent of the author(s) and/or copyright holder(s), unless the work is under an open content license such as Creative Commons.

Takedown policy
Please contact us and provide details if you believe this document breaches copyrights.
We will remove access to the work immediately and investigate your claim.

This work is downloaded from Delft University of Technology.
For technical reasons the number of authors shown on this cover page is limited to a maximum of 10.

JOM
https://doi.org/10.1007/s11837-024-06542-1
© 2024 The Author(s)

Holistic Processing of Sawdust to Enable Sustainable Hybrid Li-Ion Capacitors

XIAOYANG GUO,[1] DICK VAN DE KLEUT,[2] JIA ZHANG,[3] CHAOFAN CHEN,[4] XUEHANG WANG,[4] TIANYE ZHENG,[3] and STEVEN BOLES [1,5]

1.—Department of Energy and Process Engineering, Faculty of Engineering, Norwegian University of Science and Technology (NTNU), Trondheim, Norway. 2.—Beyonder AS, Stokkamyrveien 30, 4313 Sandnes, Norway. 3.—Department of Electrical and Electronic Engineering, The Hong Kong Polytechnic University, Hung Hom, Kowloon, Hong Kong. 4.—Department of Radiation Science and Technology, Faculty of Applied Sciences, Delft University of Technology, Delft 2629JB, The Netherlands. 5.—e-mail: steven.boles@ntnu.no

Activated carbon has long been recognized as a promising electrode material for energy storage devices. The extraordinarily high specific area makes it challenging to replace in supercapacitors since electrical double-layer capacitors need such surfaces but also porous networks to enable electrolyte penetration. As a raw material for synthesizing activated carbon, sawdust offers key benefits, such as its renewability, abundance, favorable physical attributes for energy storage, and a more environmentally friendly synthesis process compared to mined alternative sources. In this work, electrochemical characterization is carried out which highlights the critical role of pelletization in enhancing the capacitive performance of sawdust-derived activated carbon, in addition to the implicit handling and logistical benefits. Subsequently, a Li-ion capacitor is assembled with an organic solvent-based electrolyte, sawdust-derived activated carbon serving as the positive electrode, and an Al-based foil negative electrode, potentially combining high energy and power density materials into a hybrid device. Despite commendable electrochemical performance and the use of a sustainable waste-derived positive electrode with a commoditized negative electrode, challenges remain regarding the ability to mitigate the role of surface functional groups that are stabilized by bio-carbon thermal treatments. Nevertheless, this distinctive architecture holds promise as an alternative high-power energy storage technology for a future filled with renewable energy, electric vehicles, and portable electronic devices.

INTRODUCTION

Fossil fuel consumption accounts for approximately 65% of global greenhouse gas emissions, a significant driving force behind the escalating issue of global warming.[1] To address the challenge of global warming, society's next major endeavor must involve the quest for alternative energy sources.[2] In this context, renewable energies, with their boundless supply, offer a path to environmental preservation and the long-term sustenance of our planet. However, renewables come with intermittent availability, underscoring the critical importance of energy storage systems (ESSs) in establishing an uninterrupted carbon-free energy infrastructure. ESSs play a pivotal role in enhancing the flexibility of the electrical grid, ensuring a continuous supply of energy.[3] Moreover, the evolution of more efficient and economically viable ESSs has the potential to accelerate the adoption of electric vehicles (EVs), offering a pathway to mitigate global greenhouse gas emissions. Hybrid

(Received January 15, 2024; accepted March 21, 2024)

Published online: 15 April 2024

lithium-ion capacitors (LIC) could be an intriguing technology in this landscape, offer synergistic benefits by combining a high-power capacitor positive electrode, such as activated carbon (AC), and an energy-rich, battery-type intercalation negative electrode, like graphite, integrated into the hybrid LIC device structure.[4,5] As a result, hybrid LIC stores charges through rapid ion adsorption/desorption on the positive electrode surface and simultaneous fast lithium intercalation/de-intercalation into the negative electrode host material. With an organic electrolyte used in the LIC, the operating voltage of these devices can readily pass 3.5 V. Consequently, hybrid LICs often exhibit greater power characteristics than lithium-ion batteries (LIB) and may be suitable for certain applications.[4,5]

Traditional LIB manufacturing involves complex processes like slurry mixing, coating, calendering, and vacuum drying for both electrodes. These processes result in high costs, energy consumption, and safety concerns due to chemical use. Additionally, the intricate material mixes pose supply chain challenges and ethical issues, e.g., cobalt mining in Africa.[6] In previous research, a simplified electrode design was proposed with potential sustainability benefits compared to conventional methods.[7] By prelithiating an Al foil, energy-intensive heating and drying steps for the negative electrode may be eliminated and the usage of copper foil current collectors omitted. Such a hybrid LIC is schematically illustrated in Fig. 1. The energy can be stored via the anion adsorption onto AC positive electrode and the cation insertion into β-LiAl negative electrode.

In this study, our goal is to develop a sustainable AC positive electrode using sawdust as the precursor. The suitability of the synthesized AC is evaluated by comparing it with conventional AC electrodes which may have mining and ethical complications but are currently the best contending material for commercializing LICs. Given the notably low density of biomass feedstocks, densification becomes imperative to overcome the challenge of using a bio-derived source. Pelletization, a widely recognized and effective method for biomass densification, imparts densified and uniform shapes to biomass pellets, which eliminates powder handling from the logistical handling of sawdust. However, pellitization will potentially influence the reaction during the different stages of the activation process. Consequently, this work considers the impact of pelletization during physical activation on the performances as a hybrid LIC positive electrode.

EXPERIMENTAL SECTION

Materials

All chemicals were used as received without further treatment unless otherwise indicated.

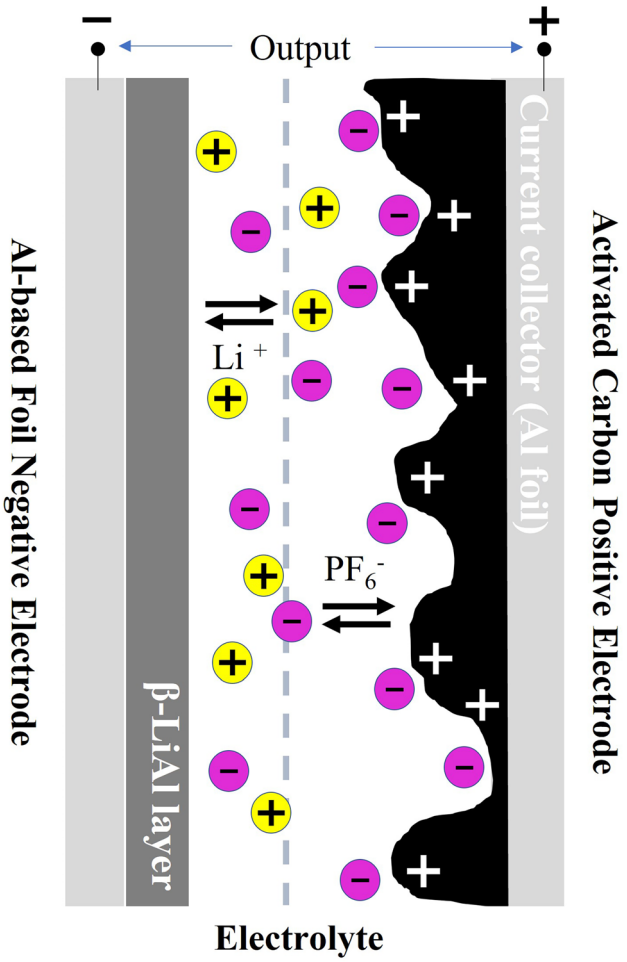


Fig. 1. Schematic illustration of an LIC with the Al-based foil negative electrode and the activated carbon positive electrode.

Sawdust-derived intermated activated carbon (iAC) was obtained from Beyonder AS in Sandnes, Norway. SUPER C45 Carbon Black was obtained from MTI. Aluminum foils (0.18 mm thick) were obtained from Toyo Aluminium K.K. The separator used in the LICs was a monolayer microporous membrane (25 μm thick, Celgard 2400). Polytetrafluoroethylene binder (PTFE, 60 wt.% dispersion in H_2O) and 1 M $LiPF_6$ in EC:DMC 1:1 vol% electrolyte were purchased from Sigma-Aldrich.

Carbon Activation Procedures and Positive Electrode Fabrication

The as-received sawdust was divided into three categories: (1) original state, (2) 4-mm pellets, and (3) 6-mm pellets. The three samples underwent identical chemical and physical activation processes. Phosphoric acid chemical activation processes and subsequent washing of the intermediate activated carbon samples were conducted at Beyonder AS. The intermediate activated carbon (iAC) obtained after chemical activation was transferred to a horizontal tubular furnace and physically activated at temperatures of 700°C, 800°C, and

900°C for 30 min under a CO_2 atmosphere, employing a heating and cooling rate of 10°C min^{-1}. All the final AC was ball milled for 10 h to obtain a powder with a particle size < 30 μm. The as-prepared AC samples are listed below in Table I.

Self-standing electrodes were prepared by mixing 87 wt.% AC powder, 8 wt.% PTFE binder (10 wt.% dispersion in H_2O), and 5 wt.% SUPER C45 Carbon Black into a dough and roll pressed at 80°C with the aid of a hot rolling machine from MTI. AC electrodes with a thickness of 50 μm were obtained after the calendaring process; 12 mm disks were punched from the laminated electrode, weighed, and dried overnight in a vacuum oven at 140°C. The thickness of the active material was 50 μm, and the mass loading of AC was 3.5 mg/cm^2.

Aluminum Foil-Based Negative Electrode Synthesis

The Al foil is punched into 12-mm disks; 5 μL of liquid electrolyte is placed between an Al disk ($\sim$ 55 mg) and a Li metal disk ($\sim$ 4.8 mg). Upon assembly, the prelithiation process effectively starts immediately, referring to electrolyte-mediated lithiation.[31] This prelithiation is done in an argon-filled glove box, where water and oxygen concentrations were < 0.1 ppm. Afterward, the Al foil-based negative electrode is ready to be paired with the AC positive electrode in a CR2032-coin cell format.

Material Characterization

The morphology of the samples was revealed using a Zeiss Ultra 55 LE thermal field emission gun scanning electron microscope (FEG-SEM) operated at 10 kV.

Thermogravimetric analyses were carried out by using a TGA-MS (TGA: Netzsch STA 449C Jupiter, MS: Netzsch Aërlos QMS 403C, Netzsh Group, Selb, Germany) to qualify and quantify the oxygen-containing functional groups on the AC surface. A mixture of Ar purge (flow of 60 cm^3/min) and protective Ar gas (flow of 20 cm^3/min) was applied. Ten milligrams of AC samples was heated starting from room temperature to 1100°C with a heating rate of 5°C/min. The evaluation encompasses the examination of reaction regions, peak temperatures, and mass loss of the differently sized sawdust samples. Furthermore, derivative thermogravimetric (DTG) analysis was employed to provide detailed insights into the TGA results. DTG serves to highlight key temperature regions and the corresponding rates of mass loss, offering a finer resolution in the analysis of the activated sawdust samples.

Inductively coupled plasma mass spectrometry (ICP-MS) was conducted using a High-Resolution Inductively Coupled Plasma Element 2 in combination with an ICP-MS triple quad Agilent 8800. Approximately 0.250 g accurately weighed AC samples was microwave digested by Milestone UltraClave 3 with concentrated nitric acid (HNO_3, 2 mL, 65%). The final solutions were diluted with deionized water and filled into a 16-mL sample.

X-ray diffraction (XRD) was performed in a homemade airtight electrochemical cell with a beryllium window[8] acting as a current collector allowing X-rays to easily penetrate. The airtight electrochemical cell was assembled in the argon-filled glovebox.

Electrochemical Characterization

The 2032-type coin cells were assembled with AC as the working electrode Li foils as the counter electrode for half-cells and in situ prelithiated Al foils as the counter electrode for full-cells. Celgard 2400 and 1 M LiPF6 in EC:DMC 1:1 vol.% were used as the separator and electrolyte, respectively. Galvanostatic charge and discharge (GCD) measurements were performed at room temperature using an eight-channel battery analyzer (LAND CT3002A). The voltage range was 2.0–3.6 V for both half cells and full cells. The rate capability of cells was tested at different current densities (0.25 mA cm^{-2}, 0.5 mA cm^{-2}, 1 mA cm^{-2}, 2 mA cm^{-2}, 5 mA cm^{-2}, 10 mA cm^{-2}).

Table I. AC samples prepared by sawdust with different pellet sizes and at different activation temperatures

	CO_2 activation temperature	Final AC samples
Original sawdust	700	AC-OS-700
	800	AC-OS-800
	900	AC-OS-900
4-mm pellets	700	AC-4 mm-700
	800	AC-4 mm-800
	900	AC-4 mm-900
6-mm pellets	700	AC-6 mm-700
	800	AC-6 mm-800
	900	AC-6 mm-900

RESULTS AND DISCUSSION

Activated Carbon Characterization

The scanning electron microscopy (SEM) images of sawdust-derived AC before and after the ball milling process are presented in Fig. 2. Figure 2a illustrates that the overall structure of the AC sample before the ball milling process, and Fig. 2b highlights a wall thickening phenomenon: The cell wall of wood, which was quite thin (red dashed line), becomes significantly thicker after the activation process.[8] In short, it largely maintains the honeycomb structure of wood cells but with much thicker cell walls. Similar honeycomb structures have been identified in the AC derived from biomass precursors by others,[9–12] and such honeycomb-like hierarchical porous morphology is presumed to benefit high charge-discharge performance in capacitors.[12] The disruption of the original wall structure of the wood during ball milling results in a more uniform particle size distribution of the AC (Fig. 2c and d), and these particles can be utilized in the synthesis of a self-standing electrode for the hybrid Li-ion capacitor.

Normally, the yield of the activation process in the production of AC provides crucial insights into production efficiency, resource utilization, and product quality. The yields of the physical activation step for the prepared AC samples are presented in supplementary Table S-I (refer to online supplementary material), calculated based on the weight change before and after CO_2 activation at 700°C, 800°C, and 900°C. The yields of the physical activation step were lower at higher activation temperatures because of the increased reaction rate of CO_2 and carbon. Also, the yields were slightly higher for samples with larger particle sizes, probably because of diffusion limitations during the activation process. This refers to the necessity for gases like CO_2 and CO to diffuse through the surface and pores of intermediate activated carbon, which is more pronounced in larger particles like the 6-mm pellets. Consequently, gases must traverse longer distances before and after the reaction, potentially impacting the final yields.[13] Since surface functional groups on the surface of AC are reported to significantly elevate side reactions and leakage current,[14,15] we opted for thermogravimetric-mass-spectrometric (TGA-MS) analysis to delve deeper into their impact, particularly through the evolution of the main volatile products (H_2O, CO_2, CO, SO_2).

Figure 3 shows that, compared to the original sawdust (AC-OS-800), densification by shaping into 4-mm (AC-4 mm-800) and 6-mm (AC-6 mm-800) pellets brings about slight modifications to the pyrolysis of the precursor as shown in supplementary Fig. S-I. With the increase of densification from the original sawdust to 6-mm pellets and further to 4-mm pellets, the weight loss stages shifted to a slightly higher temperature. Also, the data of the AC sample obtained by CO_2 activation of 4-mm pellet precursor at 900°C (AC-4 mm-900) are

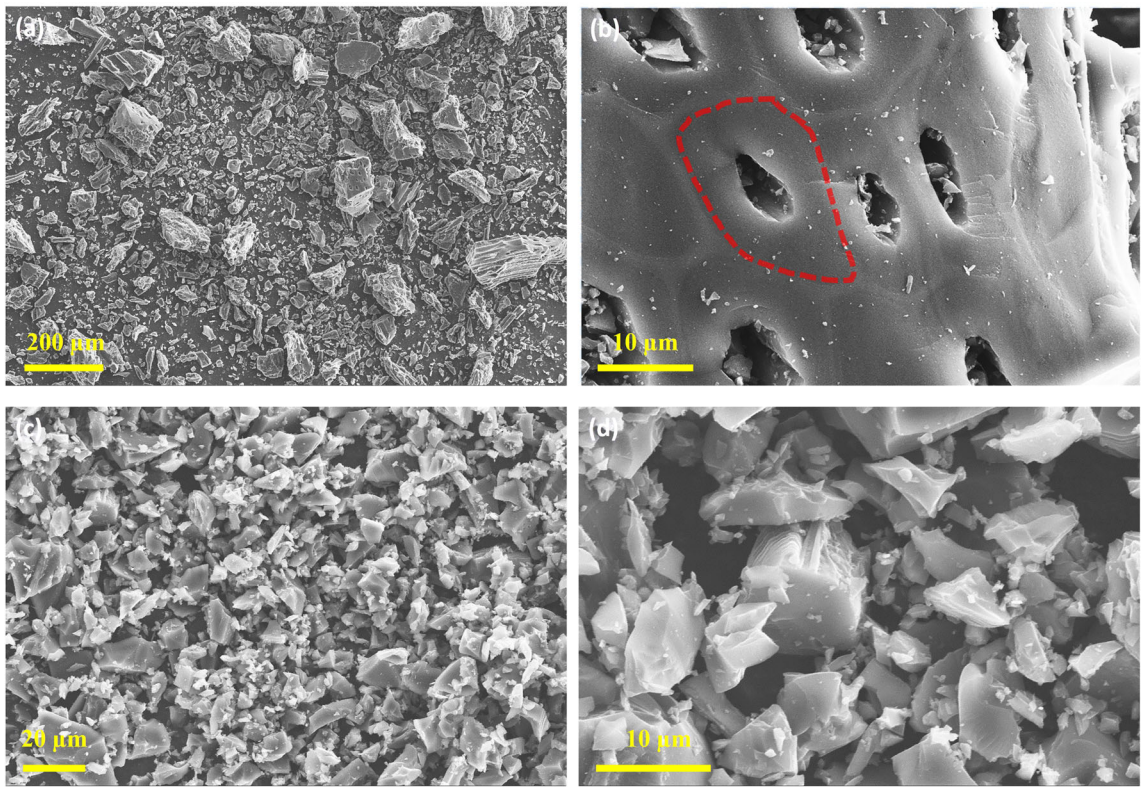


Fig. 2. SEM images of AC-4 mm-900: (a), (b) before and (c), (d) after the ball mill process.

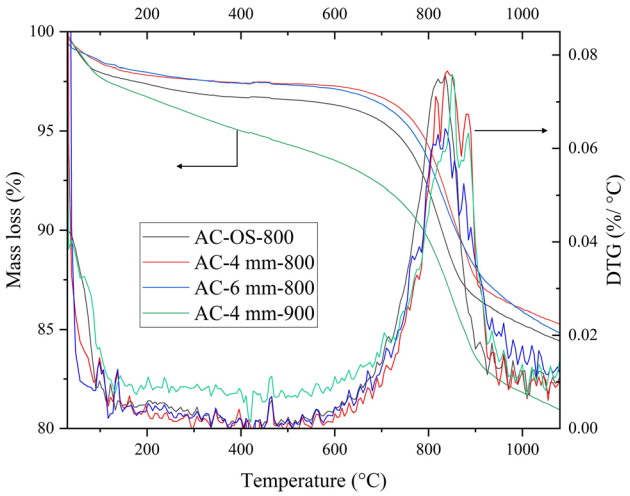


Fig. 3. TGA-DTG of AC with different pellet sizes subjected to CO_2 activation at temperatures of 800°C or 900°C: original sawdust at 800°C (black), 4 mm at 800°C (red), 6 mm at 800°C (blue), and 4 mm at 900°C (green) at a heating rate of 5°C/min (Color figure online).

presented in the figure. This sample exhibits slightly higher weight loss at lower temperatures compared to the three samples activated at 800°C. However, the DTG profile of (AC-4 mm-900) still peaks at higher temperatures, indicating that its main weight loss occurs at relatively higher temperatures. Perhaps this is statistically insignificant and requires further detailed experiments to understand the role of macro-densification (i.e., pelletization) and activation temperature on the pyrolysis process.

Supplementary Fig. S-I shows that the surface-adsorbed water vapor, CO, and CO_2 on all AC samples rapidly desorb from the sample surfaces shortly after the commencement of the test. Gaseous emissions occur at the temperature interval between 600°C and 1000°C, simultaneously with mass degradation (DTG profile). A green dashed line at 800°C was added to supplementary Fig. S-I, which serves as a reference point for comparing the peaks of product evolutions from the different samples. By comparing the curves in Fig. 4, which illustrates the case of loosely activated sawdust samples (i.e., without a pelletizing step), a substantial amount of CO is released at temperatures just above 800°C. Both the pelletization process and increasing the physical activation temperature appear to elevate the temperature at which CO is released, accompanied by a reduction in the quantity of released CO. A similar trend is observed for CO_2, but the influence on H_2O is comparatively less pronounced. This might be attributed to enhanced contact with phosphoric acid and gas flow in both chemical and physical activation processes. In the case of loosely activated sawdust samples without the pelletizing step, it is anticipated that more reactive sites on their surface would be generated after preparation. Consequently, this likely resulted in the formation of a greater number of functional groups, leading to increased CO and CO_2 generation during TGA analysis. One supporting explanation for this phenomenon would be that the surface of loosely activated sawdust is more accessible to air, leading to a slightly higher degree of oxidation.

The results of ICP-MS are shown in supplementary Table S-II. There are large differences in the amounts of impurities between the reference commercial activated carbon (REF) and the sawdust-derived AC. In comparison, the latter exhibits higher concentrations of both metallic and non-metallic elements. The exceptionally elevated phosphorus content suggests a need for intensified washing processes to eliminate excess phosphoric acid,[16] which affects the initial carbonization and porosity evolution.[17,18] When the sawdust-derived AC is pelletized, higher levels of metallic elements, such as iron (Fe), aluminum (Al), chromium (Cr), and nickel (Ni), can be expected likely because of friction and compression with the metal components in the machinery. Subsequent washing procedures are therefore needed to remove these metallic impurities to meet the commercial standard and thus to achieve better electrochemical performance.[19,20]

Electrochemical Performance Assessment

Half-cell configuration (Li//AC) and a voltage range of 2.0–3.6 V (versus Li/Li^+) are used to characterize the sawdust-derived AC electrodes. The galvanostatic charge-discharge (GCD) is conducted with the current densities of 0.25 mA cm^{-2}, 0.5 mA cm^{-2}, 1 mA cm^{-2}, 2 mA cm^{-2}, 5 mA cm^{-2}, and 10 mA cm^{-2}. Figure 5 shows the coulombic efficiency (a) and rate performance (b) of the AC electrodes prepared from the sawdust pellet precursors with different sizes and activated in CO_2 atmosphere at 800°C or 900°C for 30 min. The coulombic efficiency of the half-cell using the AC electrode is presented in Fig. 5a. The electrodes crafted from 4-mm sawdust pellets (AC-4 mm-800 and AC-4 mm-900) exhibit the highest level of stability in coulombic efficiency, approaching 100% compared to their counterparts. The areal capacities of the three AC electrodes remain more or less the same level at the low current density (0.25 mA cm^{-2}), as shown in Fig. 5b. However, the half-cells obtained from electrodes made with original sawdust (AC-OS-800) and 6-mm sawdust pellets (AC-6 mm-800) exhibit a rapid decline when the current density becomes larger, approaching zero at a current density of 10 mA cm^{-2}. Moving on to AC-4 mm-800 and AC-4 mm-900, there are distinct improvements in areal capacity and rate capability.

Oxygen functional groups are reported to negatively affect the stability of carbon-based electrodes when in contact with electrolyte.[19,21–23] The oxygen-containing functional groups often serve as active sites which may catalyze the decomposition of the

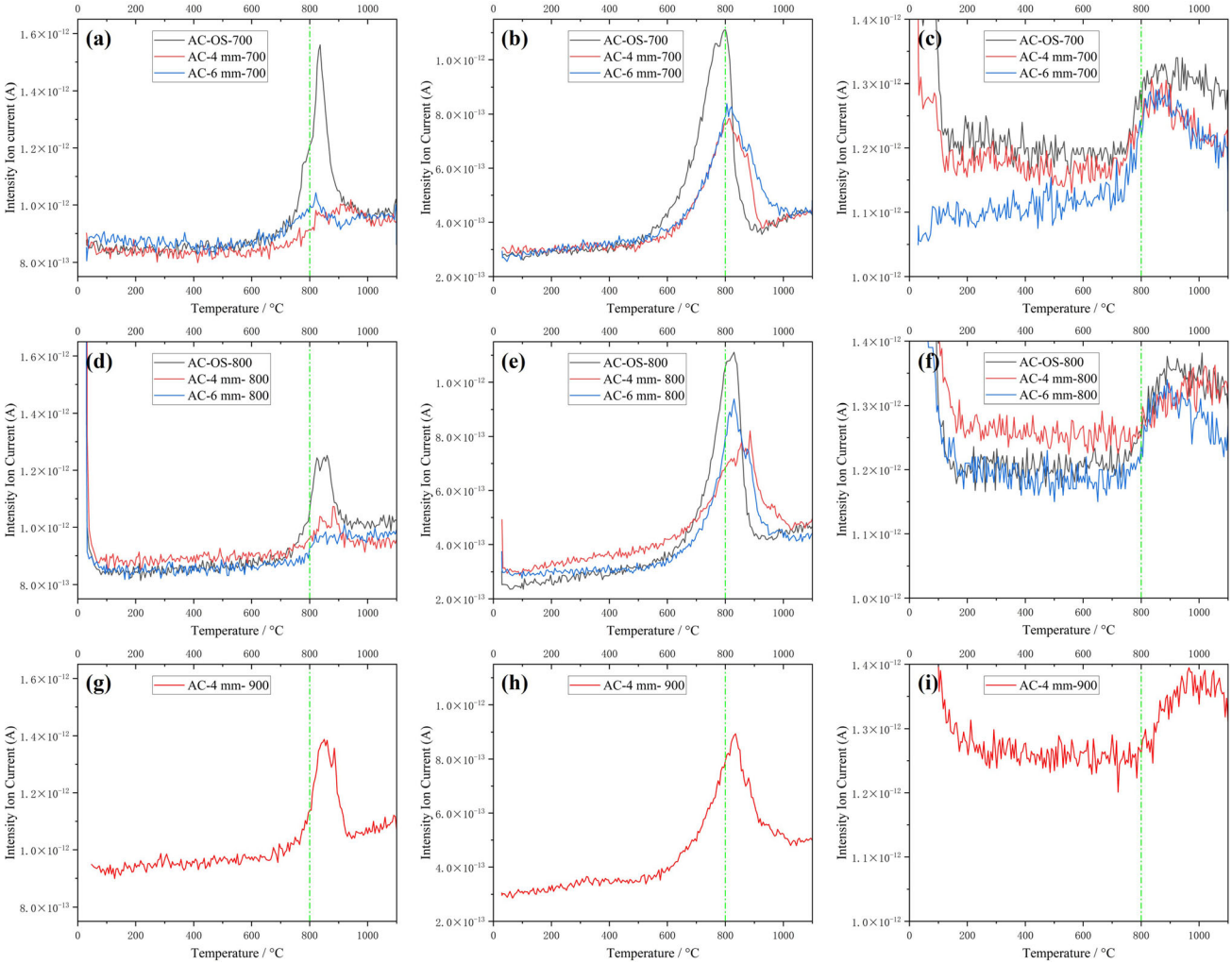


Fig. 4. Comparison of single gas (CO: a, d, and g; CO_2: b, e, and h; H_2O: c, f, and i) released from TGA-MS of AC with different pellet sizes and subjected to CO_2 activation at temperatures of 700°C (a, b, and c), 800°C (c, d, and e), and 900°C (g, h, and i).

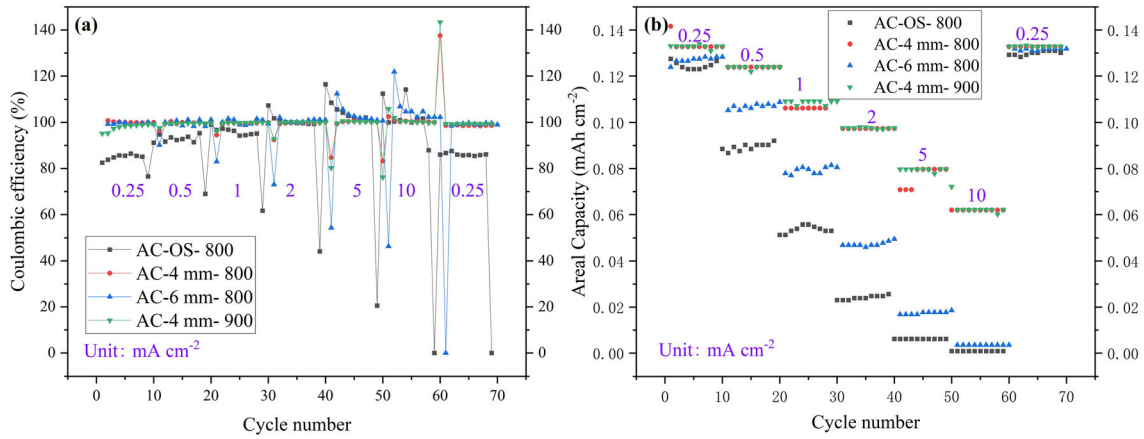


Fig. 5. Comparison of coulombic efficiency (a) and rate capability (b) of half-cells with carbon materials from different pellet sizes at different current densities. Carbon materials were activated in CO_2 atmosphere at 800°C or 900°C for 30 min.

electrolyte components and/or the electrochemical reduction or oxidation of carbon.[24] The experimental findings from other research indicate that the presence of surface oxygen functional groups on AC leads to a reduction in the surface conductivity.[24–26] Moreover, specific simulation results have indicated

that the introduction of oxygen functional groups into the pores of AC can impede ion transport to the pores, consequently lowering the current density in regions of the activated carbon where oxygen functional groups are present.[24,25,27] These accumulated effects substantially contribute to an increased equivalent series resistance (ESR) observed in hybrid LIC devices.[25] Notably, the leakage current of hybrid LIC devices poses a significant bottleneck issue in practical applications,[28] with ion desorption driven primarily by ion concentration gradient and potential field identified as the root cause.[29] The involvement of oxygen-containing functional groups on carbon materials in ion desorption is particularly noteworthy.[28] Therefore, the removal of oxygen-containing functional groups from the AC electrode should positively affect the performance of our hybrid LIC device.[22,30] The argument seems to agree with the TGA-MS results, which indicate that the AC derived from 4-mm pellets contains the least amount of these surface functional groups and gives the best electrochemical performances. Our half-cell testing reveals that when AC surfaces feature a substantial presence of oxygen-containing functional groups, the areal capacity significantly decreases at higher current densities. Therefore, it is advisable to use AC with minimal or no such oxygen-containing functional groups in scenarios with elevated current density.

In summary, the pelletization processes seem to notably impact the surface functional groups and the electrochemical performance of the sawdust-derived AC electrodes. The rate performance of half-cells, using different-sized sawdust pellets, indicates varying coulombic efficiency and areal capacity. The TGA-DTG analysis highlights the influence of pellet size on pyrolysis. Furthermore, CO_2 activation at three temperatures produced distinct gas release patterns, with the weight loss stages shifting to slightly higher temperatures when sawdust was densified through pelletization. The diverse yields observed at different temperatures suggest varying activation levels, leading to a range of porosities in AC, consequently resulting in distinct surface areas and pore volumes. Additionally, the study emphasizes the importance of addressing oxygen functional groups for improved stability of the AC electrode in hybrid capacitor applications.

Aluminum-Based Foil Negative Electrode

The other crucial factor facilitating this demonstration is the aluminum-based foil negative electrode, created by electrolyte-mediated mechanical prelithiation of aluminum metal foil.[31] With the quantity of Li metal used, it is expected to give rise to a 160-μm β-LiAl layer on the Al foil. Figure 6a shows the X-ray diffractograms for the pristine Al foil and the foil after 10 h of lithiation, which clearly show the crystalline β-LiAl (cubic, PDF: JCPDS 03-1215, lattice constant: a = 0.6373 nm) and the Al peaks. A slight shift of the Al peaks can be observed after lithiation, and this is probably due to the mechanical stress that stains the neighboring Al grains.[32,33] Open-circuit voltage (OCV) monitoring of the lithiation process in a half-cell configuration is presented in Fig. 6b, in which the OCV stabilized at $\sim$ 342 mV, which is very close to the equilibrium potential of the β-LiAl, indicating β-LiAl was formed on top of Al foil.[32,34] The combination of the observed LiAl presence in XRD results and the stable OCV of $\sim$ 360 mV[35] after 10 h leads to the inference that the lithiation process is completed at this point.

Device Performance Assessment

The feasibility and overall characteristics of a hybrid LIC rechargeable cell utilizing sawdust-derived AC as the positive electrode and an electrolyte-mediated in situ lithiated Al-based foil negative electrode should be electrochemically assessed further. Figure 7a and b depicts the rate capability and coulombic efficiency of the hybrid LIC using the AC-4 mm positive electrodes, which were activated by CO_2 at different temperatures. It is observed that the hybrid LIC cell assembled with AC-4 mm-900 maintains approximately 85% of its capacity when increasing the current from 0.25 mAh cm^{-2} to 2 mAh cm^{-2}. This rate performance can result in a $\sim$ 6.8 times higher power density (calculated as 8 times 85%), emphasizing the superior rate capability within this specified current range. However, for the hybrid LICs assembled with carbon materials activated at 700°C and 800°C, the rate capability and coulombic efficiency are not as good as the one activated at 900°C. Then, the hybrid LIC assembled with AC-900 was selected for the galvanostatic charge-discharge test and long-term cycling performance test; the results are presented in Fig. 7c and d. The galvanostatic profiles show an ideal symmetry between charge and discharge under all selected current densities Nevertheless, as the rate is further increased, there is a dramatic decrease in capacity. Hence, the assessment of cycling performance occurs at 2 mA cm^{-2}, where a balance between energy and power density aligns with expected application requirements. As illustrated in Fig. 7d, the hybrid LICs exhibit their highest areal capacity after approximately 300 cycles, maintaining about 95% capacity retention after 1000 cycles. Given that the cycled capacity is constrained by the positive electrode, the negative electrode material can leverage the Li solubility range of β-LiAl, allowing for (de-)lithiation without altering its crystal structure. In contrast to the limited cycling durability observed in Al negative electrodes as reported by others,[36–38] our devices capitalize on the solubility range of β-LiAl, effectively mitigating inherent issues associated with phase transformations, including the formation of nanopores and mechanical strain.

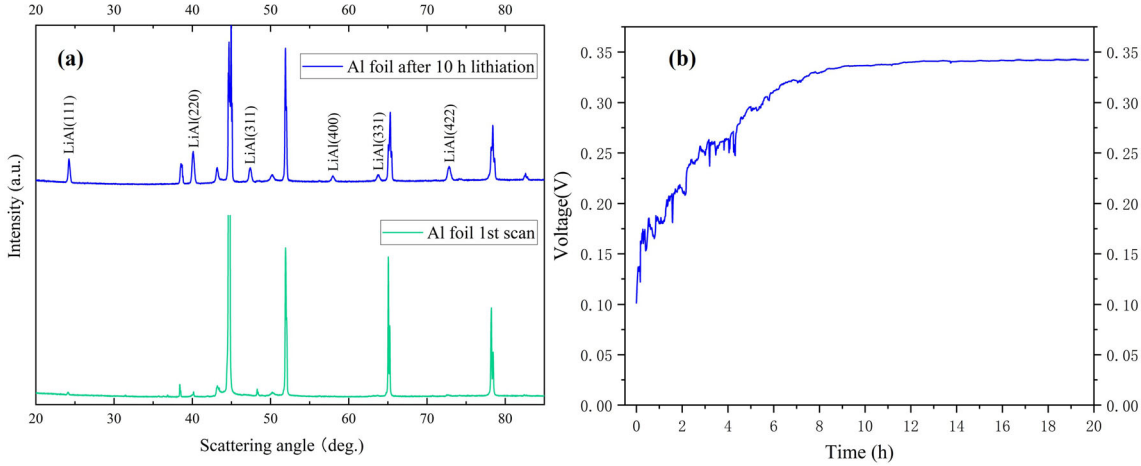


Fig. 6. Electrolyte-mediated in situ lithiated Al foil negative electrode: (a) XRD pattern of the Al foil at the start of the lithiation process and after 10 h lithiation, (b) OCV monitoring of the lithiation process in a half cell configuration.

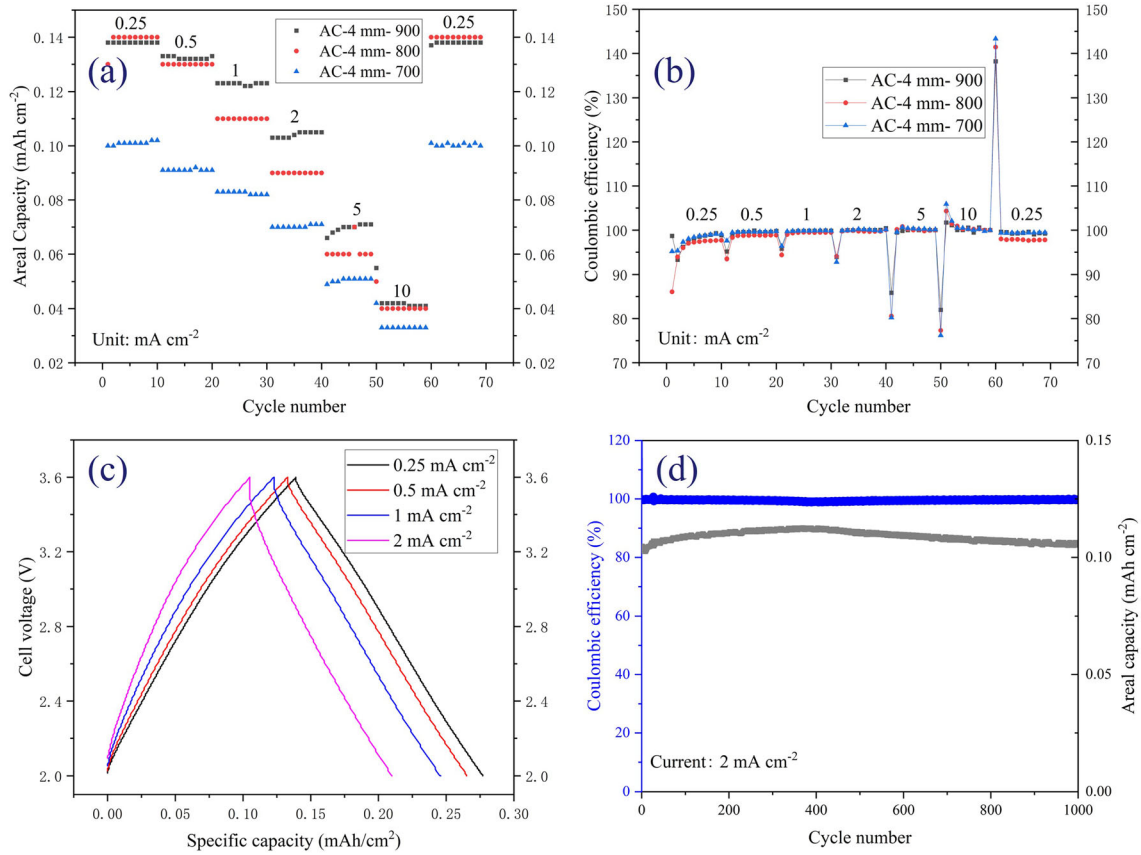


Fig. 7. Comparison of rate capability (a) and coulombic efficiency (b) of electrodes made from carbon materials from 4 mm sawdust pellets activated by CO_2 at different temperatures and at different current densities. (c) Galvanostatic charge-discharge curves of a hybrid LIC consisting of in situ lithiated Al foil negative electrode and the 900°C AC negative electrode at different current densities and (d) cycling performance at 2 mA cm^{-2}.

CONCLUSION

In summary, this study assesses the suitability of AC derived from sawdust as the positive electrode for a hybrid LIC. Together with an Al-based foil negative electrode, the simplicity of the electrode fabrication process, coupled with the elimination of traditional energy-intensive assembly steps, positions this design as a more environmentally friendly alternative to ones made using conventional methods. The AC positive electrode, produced through a green synthesis approach, addresses concerns related to contaminant release during conventional

production. The electrochemical characterization of the electrode materials highlights their potential for energy storage applications. The assembly of a high-performance hybrid LIC further validates the technical feasibility of the proposed electrode configuration. The observed electrochemical performance, coupled with the sustainability benefits, positions the sawdust-derived AC positive and Al-based foil negative electrode as a promising combination for future energy storage devices. Nevertheless, challenges persist in mitigating the impact of surface functional groups on the surface of bio-carbons. Addressing these challenges is crucial for bridging the gap between our innovative approach and the performance disparities observed in commercial AC products.

SUPPLEMENTARY INFORMATION

The online version contains supplementary material available at https://doi.org/10.1007/s11837-024-06542-1.

ACKNOWLEDGEMENTS

This work was supported by the Research Council of Norway (NFR) for funding under project number 332081. Xiaoyang Guo gratefully acknowledges the support from Beyonder AS and helpful technical discussions with Dr. Markus Solberg Wahl at NTNU, and Kingsley Ugochukwu, Jacob Ponniah at Beyonder AS. Tianye Zheng gratefully acknowledges the 'PolyU Distinguished Postdoctoral Fellowship Scheme' (1-YWBT) and the support from Professor Wei Jin at The Hong Kong Polytechnic University (PolyU). Jia Zhang acknowledges the support from the Teaching Postgraduate Studentship (TPS) Scheme from Department of Electrical and Electronic Engineering at The Hong Kong Polytechnic University (PolyU). Xiaoyang Guo, Jia Zhang and Steven T Boles acknowledges the ENERSENSE research initiative (68024013) at Norwegian University of Science and Technology (NTNU), Norway. The authors are thankful to Toyo Aluminium K.K., Japan for providing the Al foil samples.

FUNDING

Open access funding provided by NTNU Norwegian University of Science and Technology (incl St. Olavs Hospital - Trondheim University Hospital).

CONFLICT OF INTEREST

On behalf of all authors, the corresponding author states that there is no conflict of interest.

OPEN ACCESS

This article is licensed under a Creative Commons Attribution 4.0 International License, which permits use, sharing, adaptation, distribution and reproduction in any medium or format, as long as you give appropriate credit to the original author(s) and the source, provide a link to the Creative Commons licence, and indicate if changes were made. The images or other third party material in this article are included in the article's Creative Commons licence, unless indicated otherwise in a credit line to the material. If material is not included in the article's Creative Commons licence and your intended use is not permitted by statutory regulation or exceeds the permitted use, you will need to obtain permission directly from the copyright holder. To view a copy of this licence, visit http://creativecommons.org/licenses/by/4.0/.

REFERENCES

1. V. Masson-Delmotte, P. Zhai, H.-O. Pörtner, D. Roberts, J. Skea, and P.R. Shukla, *Global Warming of 1.5 C: IPCC Special Report on Impacts of Global Warming of 1.5 C Above Pre-industrial Levels in Context of Strengthening Response to Climate Change, Sustainable Development, and Efforts to Eradicate Poverty* (Cambridge University Press, 2022).
2. J. Ajuria, E. Redondo, M. Arnaiz, R. Mysyk, T. Rojo, and E. Goikolea, *J. Power. Sources* 359, 17 https://doi.org/10.1016/j.jpowsour.2017.04.107 (2017).
3. P. Denholm, E. Ela, B. Kirby, and M. Milligan, National Renewable Energy Lab. (NREL), Golden, CO (United States) (2010).
4. M. Soltani and S.H. Beheshti, *J. Energy Storage* 34, 102019 https://doi.org/10.1016/j.est.2020.102019 (2021).
5. W. Zuo, R. Li, C. Zhou, Y. Li, J. Xia, and J. Liu, *Adv. Sci. (Weinh)* 4, 1600539 https://doi.org/10.1002/advs.201600539 (2017).
6. F.K. Crundwell, N.B. du Preez, and B.D.H. Knights, *Miner. Eng.* 156, 106450 https://doi.org/10.1016/j.mineng.2020.106450 (2020).
7. T. Zheng and S.T. Boles, *ACS Omega* 7, 37867 https://doi.org/10.1021/acsomega.2c04966 (2022).
8. M. Jagtoyen and F. Derbyshire, *Carbon* 36, 1085 https://doi.org/10.1016/S0008-6223(98)00082-7 (1998).
9. M. Sivachidambaram, J.J. Vijaya, L.J. Kennedy, R. Jothiramalingam, H.A. Al-Lohedan, M.A. Munusamy, E. Elanthamilan, and J.P. Merlin, *New J. Chem.* 41, 3939 https://doi.org/10.1039/C6NJ03867K (2017).
10. B. Viswanathan, P.I. Neel, and T. Varadarajan, *India Chennai* 600, 1 (2009).
11. M. Dutta, S. Mishra, M. Kaushik, and J.K. Basu, *Res. J. Environ. Sci.* 5, 741 https://doi.org/10.3923/rjes.2011.741.751 (2011).
12. S.P. Hou, M.D. Liao, C. Peng, D. Min, X.Y. Li, J. Chen, G.T. Yu, and J.H. Lin, *Energy Fuels* 35, 16860 https://doi.org/10.1021/acs.energyfuels.1c01690 (2021).
13. T. Mani, P. Murugan, J. Abedi, and N. Mahinpey, *Chem. Eng. Res. Des.* 88, 952 https://doi.org/10.1016/j.cherd.2010.02.008 (2010).
14. P. Azaïs, L. Duclaux, P. Florian, D. Massiot, M.-A. Lillo-Rodenas, A. Linares-Solano, J.-P. Peres, C. Jehoulet, and F. Béguin, *J. Power. Sources* 171, 1046 https://doi.org/10.1016/j.jpowsour.2007.07.001 (2007).
15. Y. An, C. Li, X. Sun, K. Wang, F. Su, F. Liu, X. Zhang, and Y. Ma, *J. Phys. D Appl. Phys.* 55, 045501 https://doi.org/10.1088/1361-6463/ac2db3 (2021).

16. H. Hadoun, Z. Sadaoui, N. Souami, D. Sahel, and I. Toumert, *Appl. Surf. Sci.* 280, 1 https://doi.org/10.1016/j.apsusc.2013.04.054 (2013).
17. B.S. Girgis and A.N.A. El-Hendawy, *Microporous Mesoporous Mater.* 52, 105 https://doi.org/10.1016/S1387-1811(01)00481-4 (2002).
18. P.J.M. Carrott, M.M.L.R. Carrott, and P.A.M. Mourao, *J. Anal. Appl. Pyrol.* 75, 120 https://doi.org/10.1016/j.jaap.2005.04.013 (2006).
19. I. Piñeiro-Prado, D. Salinas-Torres, R. Ruiz-Rosas, E. Morallón, and D. Cazorla-Amorós, *Front. Mater.* 3, 16 https://doi.org/10.3389/fmats.2016.00016 (2016).
20. K. Kierzek and G. Gryglewicz, *Molecules* 25, 4255 https://doi.org/10.3390/molecules25184255 (2020).
21. T. Zhang, B. Fuchs, M. Secchiaroli, M. Wohlfahrt-Mehrens, and S. Dsoke, *Electrochim. Acta* 218, 163 https://doi.org/10.1016/j.electacta.2016.09.126 (2016).
22. A.G. Pandolfo and A.F. Hollenkamp, *J. Power. Sources* 157, 11 https://doi.org/10.1016/j.jpowsour.2006.02.065 (2006).
23. S. Liu, S. Liu, K. Huang, J. Liu, Y. Li, D. Fang, H. Wang, and Y. Xia, *J. Solid State Electrochem.* 16, 1631 https://doi.org/10.1007/s10008-011-1573-7 (2012).
24. C.T. Hsieh and H. Teng, *Carbon* 40, 667 https://doi.org/10.1016/S0008-6223(01)00182-8 (2002).
25. Y.T. He, Y.H. Zhang, X.F. Li, Z. Lv, X.J. Wang, Z.G. Liu, and X.Q. Huang, *Electrochim. Acta* 282, 618 https://doi.org/10.1016/j.electacta.2018.06.103 (2018).
26. C.J. Qiu, L.L. Jiang, Y.G. Gao, and L.Z. Sheng, *Mater. Des.* 230, 111952 https://doi.org/10.1016/j.matdes.2023.111952 (2023).
27. H.Y. Liu, H.H. Song, X.H. Chen, S. Zhang, J.S. Zhou, and Z.K. Ma, *J. Power. Sources* 285, 303 https://doi.org/10.1016/j.jpowsour.2015.03.115 (2015).
28. W. Li, X.M. Yang, Z.M. Chen, X.F. Wang, and J.S. Qiu, *Carbon* 196, 136 https://doi.org/10.1016/j.carbon.2022.04.037 (2022).
29. K.L. Liu, C. Yu, W. Guo, L. Ni, J.H. Yu, Y.Y. Xie, Z. Wang, Y.W. Ren, and J.S. Qiu, *J. Energy Chem.* 58, 94 https://doi.org/10.1016/j.jechem.2020.09.041 (2021).
30. Y.T. Ju, M.Y. Cho, M.H. Kim, J.W. Lee, S.M. Park, B.H. Choi, and K.C. Roh, *J. Ceram. Process. Res.* 13, S159 (2012).
31. J. Ryu, J. Kang, H. Kim, J.H. Lee, H. Lee, and S. Park, *Energy Storage Mater.* 33, 164 https://doi.org/10.1016/j.ensm.2020.08.012 (2020).
32. T.Y. Zheng and S.T. Boles, *Progress Energy*. https://doi.org/10.1088/2516-1083/acd101 (2023).
33. T. Zheng, D. Kramer, M.H. Tahmasebi, R. Monig, and S.T. Boles, *Chemsuschem* 13, 5910 https://doi.org/10.1002/cssc.202002023 (2020).
34. T. Zheng, D. Kramer, R. Mönig, and S.T. Boles, *ACS Sustain. Chem. Eng.* 10, 3203 https://doi.org/10.1021/acssuschemeng.1c07242 (2022).
35. H.T. Jeong, J. Jang, D.G. Lee, D. Lee, and W.J. Kim, *J. Alloys Compd.* 965, 171279 https://doi.org/10.1016/j.jallcom.2023.171279 (2023).
36. G. Oltean, C.W. Tai, K. Edström, and L. Nyholm, *J. Power. Sources* 269, 266 https://doi.org/10.1016/j.jpowsour.2014.06.118 (2014).
37. S.K. Sharma, M.S. Kim, D.Y. Kim, and J.S. Yu, *Electrochim. Acta* 87, 872 https://doi.org/10.1016/j.electacta.2012.09.028 (2013).
38. N. Hudak and D. Huber, *ECS Trans.* 33, 1 https://doi.org/10.1149/1.3557706 (2011).

Publisher's Note Springer Nature remains neutral with regard to jurisdictional claims in published maps and institutional affiliations.